# Simulation of diffuse, constricted-stratified, and constricted modes of a dc discharge in argon: Hysteresis transition between diffuse and constricted-stratified modes

I. A. Shkurenkov, Yu. A. Mankelevich, and T. V. Rakhimova
*Skobeltsyn Institute of Nuclear Physics, Lomonosov's Moscow State University, Leninskie Gory, Moscow 119991, Russia*
(Received 19 January 2009; published 27 April 2009)

This paper presents the results of theoretical studies of high-pressure $p$ (tens and hundreds of Torr) direct current (dc) discharges in argon. The diffuse (D), constricted-stratified (CS), and constricted (C) discharge modes are studied using a developed one-dimensional (radial) model. The model includes the conservation equations for electrons, ions ($Ar^+$ and $Ar_2^+$), and excited atoms (metastable and resonant states) for mean electron energy and for the temperature of the high-energy part of the electron-energy distribution function (EEDF), the heat conduction equation for the neutral gas, and Poisson's equation for the radial electric field. The developed model of a dc discharge allowed us, without any artificial assumptions, to obtain periodic oscillations of plasma parameters for the CS mode and to describe a hysteresis transition between the D mode and the CS mode. Direct transition from the D to the CS mode is accompanied by an increase of several orders of magnitude in the electron density at the discharge axis and the appearance of moving striations. It was shown that the experimentally observed hysteresis of the current-voltage characteristic at the transition between the CS and D modes deals with the nonlocal formation of the EEDF, namely, the diffusion of high-energy electrons from the central constricted region. The effect of the nonlocal formation of the EEDF is taken into account by introducing the effective temperature of the high-energy part of the EEDF and solving the equation for the radial profile of this temperature. The transition from the CS mode to the C mode occurs smoothly, without any jumps of the plasma parameters. Plasma parameters and characteristics of all three modes and transitions between these modes are calculated and compared with experimental data.

DOI: 10.1103/PhysRevE.79.046406 PACS number(s): 52.65.−y, 52.25.Dg, 52.25.Jm

## I. INTRODUCTION

The phenomenon of the constriction of the positive column of a direct current (dc) discharge in inert gases at intermediate pressures (tens and hundreds of Torr) is well known in the physics of gas-discharge plasma [1] and is studied both experimentally and theoretically [1–11]. At attainment of a critical current the discharge structure and plasma parameters are changed abruptly and the discharge is compressed in a narrow bright filament. The current-voltage characteristic (CVC) of the discharge is bistable. A transition from one stable mode [diffuse (D) mode] to another [constricted (C) mode] occurs by a jump and is accompanied by an increase of several orders of magnitude in the electron density at the axis of the discharge tube. Various nonlinear mechanisms have been included in both theoretical and numerical models [9,10] to reveal the main causes resulting in constriction.

Advanced one-dimensional (1D) models describing the constriction of a high-pressure dc discharge in argon were proposed in [9,10]. These models qualitatively describe the experimentally observed variations in the plasma parameters with the discharge current I at a constant pressure and abrupt changes in these parameters at a certain critical value of the discharge current. It was shown that the combined effect of gas heating, stepwise ionization, and the influence of electron-electron collisions on the electron-energy distribution function (EEDF) resulted in discharge constriction, and all these processes and effects should be taken into account in describing the constriction phenomenon. The separate influences of these factors were also considered.

An interesting feature of the CVC during the study of the constriction in inert gases (Ne and Ar) was observed experimentally [4,6,10]. Notably, during transition from the C to the D mode, a hysteresis phenomenon [reverse curve (RC)] is observed; that is, the transition from the D mode to the C mode and the reverse transition occur at different values of the discharge current. It is significant that such RCs in the CVC were observed and analyzed in solid-state plasma (Gunn effect [12] in semiconductors and electrofield hysteresis in heterosystems [13]). However, at present there is a detailed explanation of this effect for inert gas plasma in the above mentioned models. In [10], for example, the reverse transition to the D mode was obtained in simulations at high pressure only (120 Torr) by taking into account the resonance radiative transfer. However, this mechanism turned out to be not universal. At lower pressures (40 and 80 Torr) the hysteresis transition was not obtained in simulations, contrary to the experimental data [10].

In [11], the authors of this paper showed that nonlocal effects, the so-called "memory," in the electron kinetics in radial nonuniform fields, are the reason for the S-shaped CVC (hysteresis phenomenon) at the constriction in neon. In [11], the hysteresis transition between the C and D modes was obtained, taking into account the effect of the nonlocal formation of the EEDF by introducing the effective temperature of the high-energy part of the EEDF. In the present paper, through the example of the hysteresis calculation in argon, it is shown that the proposed mechanism is universal for all inert gases. Specific features of the EEDF are revealed in the modes under study.

One more difficulty in the study of the transition between D and C modes is in the appearance of the discharge's complex structure. The presence of the negative differential conductivity in the CVC at this transition leads to the develop-

 

ment of instability. A pictorial view of ranges where the D, stratified mode without constriction (S) constricted-stratified (CS), and C modes in neon take place can be obtained from $pR$ and $I/R$ diagrams [14], $R$ is the tube radius. Similar behavior of dc discharge modes was observed in argon [14]. In the D mode of the discharge, the positive column is uniform along the tube axis. At a wide range of discharge currents (e.g., $I \approx 20-200$ mA [10,14]), constriction of the discharge is accompanied by the appearance of moving striations, which lead to modulation of plasma glowing regions (CS mode) [14]. The amplitude and frequency of the plasma local emission pulsations are decreased with the discharge current and the pulsation shape is changed from sinusoidal to substantially nonsinusoidal (in CS mode). This mode is distinct from a purely C mode and it is necessary to consider the appearance of the striations (periodic oscillations of plasma parameters). The CS mode differs greatly from the S mode. For example, in the S mode, in the region of high concentration of electrons their concentration is smoothly distributed over the cross section of the discharge tube, while in the CS mode it is concentrated in a narrow region near the discharge axis [10,15]. One can see on the diagram presented in [14] the following picture. At high pressure ($pR \geq 80$ Torr cm) the discharge can exist in three modes; they are D mode ($I/R \leq 30-50$ mA/cm), CS mode, and C mode ($I/R \geq 100-150$ mA/cm). At pressure $10 \leq pR \leq 80$ Torr cm the discharge can exist in four modes; they are D, S, CS, and C modes. The CS mode was not observed at lower pressures.

Properties of the pure striations (S mode) were studied in [16] by analyzing dispersion equations. These equations were obtained from the linearization of the original equations for the minor adjusted sinusoidal disturbance of the field proportional to $\exp i(kx-\omega t)$, where $\kappa$ is the wave vector. However, to the best of our knowledge, until now there have been no publications in which the CS mode was obtained from self-consistent simulation. In [11], where the hysteresis transition was obtained, the time dynamics was not a subject of the study: the time oscillations of the CS mode were suppressed in numerical scheme to study the peculiarities of the mechanisms of a constriction and the hysteresis transition between D and C (CS) modes.

In the present paper, it is shown that taking into account nonlocal effects in radial electric field leads to the electron concentration oscillation in an axial electric field and formation of the periodic structures with domains of high fields. Note that for more proper quantitative simulation of the CS mode (for example, the length of striations), a two-dimensional (2D) nonlocal model is necessary.

It is shown that the solution of the full set of equations (without using any time approximations) with radial disturbance in ionization rate due to nonlocal effect leads to the appearance of the plasma parameters oscillations whose structure resembles the striations [17]. The temporal distributions of charged particles and excited atoms correlate with the observed distributions of the optical emission [10]. Simulation results for D, CS, and C discharge modes and the transitions between these modes are presented. Special attention is paid to the numerical description of the hysteresis effect during a direct (at the discharge current increase) and reverse (at the current decrease) transition between D and CS modes. The disappearance of periodic oscillations of plasma parameters with the discharge current decreasing in the CS mode was observed. As the current increases, the period of oscillations is increased and the smooth transition from the CS mode to the C mode (without any jump of reduced electric field $E$) is observed at some critical current.

In Sec. II of the paper, a model of a dc discharge in argon and the basic equations are presented. The approach based on the two-temperature EEDF and the numerical methods used are described. The basic reactions and kinetic model are presented in Sec. III. Sections IV and V contain the results of modeling. Three discharge modes are described in Sec. IV. They are D, CS, and C modes. The results of simulations of the transitions between these modes are presented in Sec. V.

## II. 1D MODEL

The 1D model describing radial distributions of macroscopic plasma parameters includes the conservation equations for the densities of electrons, $Ar^+$ and $Ar_2^+$ ions, and excited atoms (in the effective metastable and resonance states), the conservation equation for electron energy, the heat conduction equation for the neutral gas, Poisson's equation for the radial electric field, and the equation for the longitudinal field at a fixed discharge current,

$$\frac{\partial n_\alpha}{\partial t} = -\nabla J^\alpha + S - L n_\alpha, \tag{1}$$

$$\frac{\partial (n_e T_e)}{\partial t} = \frac{1}{r}\frac{\partial}{\partial r}\left( r\xi n_e \frac{\partial T_e}{\partial r} + \xi J_\gamma T_e \right) + \frac{2}{3}\xi J_\alpha e E_r + \frac{2}{3}\xi \frac{n_e}{T_e}(eE_z)^2 - q_{\mathrm{el}} - q_{\mathrm{inel}}, \tag{2}$$

$$\nabla E_r = 4\pi e(n_i + n_{2i} - n_e). \tag{3}$$

Here, $n_\alpha = n_e$, $n_i$, $n_{2i}$, $n^m$, $n^r$ are the electron, atomic ion, molecular ion, metastable state, and resonance state concentrations. $J^\beta = -v_{\mathrm{dr}}^\beta n_\beta - D^\beta N_0 \nabla(n_\beta/N_0)$ is the electron and ion ($Ar^+$ and $Ar_2^+$) current density ($\beta = e, i, 2i$), $k^*$ and $k_{\mathrm{ionis}}$ are the rate coefficients for the excitation of the excited level and ionization from it, $v_{\mathrm{dr}}^\beta$ are the electron and ion drift velocities, $D^\beta$ are diffusion coefficients of electrons and $Ar^+$ and $Ar_2^+$ ions, $E_z$ and $E_r$ are the longitudinal and radial electric fields, respectively, and $J_\gamma = \frac{n_e}{T_e} e E_r + \frac{\partial n_e}{\partial r}$, $q_{\mathrm{el}}$ and $q_{\mathrm{inel}}$ are the elastic and inelastic losses. It is assumed that the frequency of elastic collisions is proportional to the electron energy: $\nu_m = a\varepsilon$ and $\xi = \frac{2}{3ma}$. For argon in the energy range of 0–16 eV, this assumption is satisfied well with $a = 1.39 \times 10^9 p$ $(\mathrm{s\ eV})^{-1}$. $T_e$ is the electron temperature.

The boundary conditions are as follows: $n_e = 0$, $n_i = 0$, and $n_{2i} = 0$ at the tube wall and $\frac{\partial n_e}{\partial t}|_{r=0} = 0$, $\frac{\partial n_i}{\partial t}|_{r=0} = 0$, and $\frac{\partial n_{2i}}{\partial t}|_{r=0} = 0$ at the axis (the condition of cylindrical symmetry). The tube wall is assumed to be kept at a constant temperature $T = 300$ K. The radial electric field at the axis is zero: $E_r|_{r=0} = 0$.

The ion mobilities were found from [2,18]: $\mu_i N = 4.83 \times 10^{18}$ $(\mathrm{cm\ s\ V})^{-1}$ and $\mu_{2i} N = 7.25 \times 10^{18}$ $(\mathrm{cm\ s\ V})^{-1}$, the electron diffusion coefficient was determined from the de-

TABLE I. List of reactions.

| | | |
|---|---|---|
| (1) Excitation | $Ar+e \rightarrow Ar^*(Ar^r)+e$ | $k_i$ ($cm^3/s$), $i=1-3$, are determined from |
| (2) Ionization | $Ar+e \rightarrow Ar^+ +e+e$ | calculated EEDF and electron cross |
| (3) Stepwise ionization | $Ar^*(Ar^r)+e \rightarrow Ar^+ +e+e$ | sections [21,22] |
| (4) Conversion | $Ar^+ +Ar+Ar \rightarrow Ar_2^+ +Ar$ | $k=1.8\times10^{-31}(300/T)^{3/4}$ ($cm^6/s$) [23] |
| (5) Dissociative recombination | $Ar_2^+ +e \rightarrow Ar^* +Ar$ | $k=4\times10^{-5}T_e^{-0.67}$ ($cm^3/s$) [24] |
| (6) Electron impact dissociation | $Ar_2^+ +e \rightarrow Ar^+ +Ar+e$ | $k=5.7\times10^{-7}$ ($cm^3/s$) [25] |
| (7) Three-body recombination | $Ar^+ +e+e \rightarrow Ar^* +e$ | $k=5.1\times10^{-9}/(T[K])^{4.5}$ ($cm^6/s$) [26] |
| (8) Radiative decay | $Ar^r \rightarrow Ar+h\nu$ | $k\approx\theta A$ ($s^{-1}$) [27] |
| (9) States mixing | $Ar^* +e \leftrightarrow Ar^r +e$ | $k\approx10^{-7}$ ($cm^3/s$) [28] |

pendence $D_e/\mu_e \sim T_e$[eV] [1], and the coefficients of ion diffusion were calculated by the formulas $D_i[cm^2/s]=3.8\times10^{-3}(T^{1.6}/p[Torr])$, $D_{2i}=5.7\times10^{-3}(T^{1.6}/p)$ [19], and for excited atoms $D^*=0.014(T^{1.7}/p)$. The electron drift velocity was determined by solving the equation for the EEDF and approximated as a function of reduced electric field $E/N$[Td; 1 Td$=10^{-17}$ V $cm^2$]: $v_{dr}=3\times10^5(E/N)^{0.265}$ for $0.3\leq E/N\leq5$ Td and $v_{dr}=10^5(E/N)$ for $E/N\geq5$ Td. In this model, only the radial drift was considered. Near the wall, where the radial field is fairly high and the accuracy in determining the ion mobility is important, the gas temperature $T$ did not exceed 350–450 K. Therefore, the ion mobility variations will be within 10% on the basis of the temperature dependence of ion mobility [20]: ion mobility at $T=800$ K decreases by 30% in comparison with that at $T=300$ K.

## III. PLASMA-CHEMICAL MECHANISM AND ELECTRON KINETICS

### A. Plasma-chemical mechanism

The plasma-chemical reactions of importance in the conditions under study and used in our model are presented in Table I. The main source of charge particles, especially in low electric fields, is the stepwise ionization [reaction (3)]. Four lower argon excited states (the 11.54 and 11.72 eV metastable and the 11.62 and 11.82 eV resonant states) were combined into two effective states (metastable $Ar^*$ and resonant $Ar^r$). These states are excited by electron impact [reaction (1)]. In the D mode, the main loss of charged particles is the diffusion transfer and its recombination on the wall. As our calculations show, $Ar_2^+$ is the main ion in this mode. The concentration and radial profile of $Ar_2^+$ are determined by the balance of ion conversion [reaction (4)], electron impact dissociation (6), and the diffusion to the wall. The main losses of charged particles in the C mode occur in the central cylindrical region as a result of dissociative recombination (5).

For plasma that is optically thick (with respect to the resonant radiation), the processes of resonance radiation transport and reabsorption should be taken into account. We used the simplified approach of the escape factor $\theta$ [27]. For typical values of the escape factor $\theta\approx10^{-4}$ in our conditions and the radiative decay rate $A=3\times10^8$ $s^{-1}$ [2], we have $\theta A\sim3\times10^4$ $s^{-1}$. The rate coefficient of the mixing of metastable and resonant levels [reaction (8)] is $k_{mix}\sim10^{-7}$ $cm^3/s$; hence, for the electron concentration in the outer regions (not in the central core) $n_e\sim3\times10^{10}$ $cm^{-3}$, we have $k_{mix}n^e\sim3\times10^3$ $s^{-1}$. As follows from these estimations, the radiation from the central hot area is absorbed in the outer regions, but outside the discharge channel the resonant levels will be radiatively deactivated rather than mixed with metastable levels and do not influence the ionization rate. So we can expect that reabsorption of the radiation at the periphery of the discharge tube can only slightly change the radial distributions of the excited atoms and charged particles.

The rate coefficients for the excitations, direct ionization, and the stepwise ionization were determined from the calculated EEDF for a given set of the electron cross sections [21,22]. It should be noted that reduced electric fields $E/N$, electron concentrations, and its radial gradients in D, CS, and C modes are varied in wide ranges and various processes and adequate approaches for electron kinetics calculations should be taken into account and used. Electron-electron collisions, which are important in CS and C modes, were also taken into account. The peculiarities of the electron temperatures and EEDF calculations in various modes are presented in Sec. III B.

Although the rate coefficients of neon and argon are rather different, the hysteresis regions in these gases under the same pressure ($pR=300$ Torr cm) take place at the similar range of the discharge current $I/R=36-43$ mA/cm for neon [2] and $I/R=33-50$ mA/cm for argon [5]. However the corresponding values of the reduced electric field are significantly different: $E/N=1.4-0.8$ Td for neon and $E/N=2.5-1.0$ Td for argon.

### B. Two-temperature EEDF: Electron-electron collisions

Electron kinetic equation for EEDF is numerically solved in two-term approach. The rate coefficients of inelastic electron-atomic reactions depend on the reduced electric field $E/N_0$ and, at a high ionization degree $n_e/N_0>10^{-5}-10^{-4}$ [11,2,29], on the electron concentrations. The rate coefficients for the gas ionization and excitation of metastable states can be obtained by solving the kinetic equation for the isotropic part $f_0$ of the EEDF while taking into account Coulomb collisions between electrons [30,11],

$$\frac{\partial f_0}{\partial t} = \frac{\mathrm{v}}{3}\mathrm{div}\left(\frac{\mathrm{v}}{\nu}\vec{\nabla} f_0 + \frac{e}{m\cdot\nu}\vec{E}\cdot\frac{\partial f_0}{\partial \mathrm{v}}\right) + \frac{e\vec{E}}{3m\cdot\mathrm{v}^2}\frac{\partial}{\partial \mathrm{v}}\left(\frac{\mathrm{v}^3}{\nu}\vec{\nabla} f_0 + \frac{\mathrm{v}^2 e\vec{E}}{m\cdot\nu}\frac{\partial f_0}{\partial \mathrm{v}}\right) - Q_{\mathrm{inel}} + \left(\frac{\delta f_0}{\delta t}\right)_{ee}. \quad (4)$$

Here, $(\frac{\delta f_0}{\delta t})_{ee}$ is the collision integral. To account for Coulomb collisions between electrons, we employ the Rosenbluth-Shkarofsky method [30].

According to our estimates, the electron-energy relaxation length $\delta$ is about 0.3 cm, which is comparable with the width of the electron density radial profile $n_e(r)$. The hot electrons can escape the central hot area, and this will change the shape of the EEDF. The shape of the EEDF at a given spatial point and therefore the excitation and ionization rate coefficients depend on the discharge plasma parameters at neighboring points. This means that it is necessary to take into account the nonlocal character of the formation of the EEDF. As shown in our model calculations [11], a transition from the C to the D mode can be regarded as a demonstration of the nonlocal character of the formation of the high-energy part of the EEDF: the diffusion of high-energy electrons (capable of producing gas ionization) from the central constricted region toward the periphery. In the nonuniform electric fields, the formation of the EEDF is described by a nonlocal kinetic equation. Under high pressures, where the total energy is not the integral of motion, the kinetic equation for the EEDF is the complex partial differential equation [31]. To take into account the nonlocal formation of the EEDF we used a two-temperature approximation for $f_0(T_e, T^*)$,

$$f_0 = \frac{2n_e}{\sqrt{\pi}T_e^{3/2}}\exp\left(-\frac{\varepsilon}{T_e}\right), \quad \varepsilon \le \varepsilon^*,$$

$$f_0 = \frac{2n_e}{\sqrt{\pi}T_e^{3/2}}\exp\left(-\frac{\varepsilon^*}{T_e} + \frac{(\varepsilon^* - \varepsilon)}{T^*}\right), \quad \varepsilon > \varepsilon^*. \quad (5)$$

We then formulated the nonlocal nonstationary equation for the effective temperature $T^*$ of the high-energy part of the EEDF, that is, the temperature of electrons with energies $\varepsilon > \varepsilon^*$, where $\varepsilon^*$ is the energy of the lowest excited state of a noble gas atom. $T_e$ characterizes the mean electron energy (the temperature of the EEDF body). The temperature $T_e$ of the low-energy part of the EEDF varies insignificantly (e.g., due to Maxwellization processes) with variations in the EEDF shape. The rate of inelastic electron-atom processes is characterized by the temperature $T^*$ of the high-energy part of the EEDF. In turn, the temperature $T^*$ is sensitive to the variation of plasma parameters $E/N$ and $n_e/N$. The integral equation for $T^*$ was obtained from the kinetic equation (4), taking into account spatial inhomogeneity [32] and electron-electron collisions [30], by integrating with the weight $\varepsilon$ and with allowance for the two-temperature character of the EEDF. Equation (6) for calculation of the $T^*(r,t)$ was derived, taking account of the electron-electron collisions and electron radial transport,

$$\frac{\partial \varphi}{\partial t} = \xi\frac{1}{r}\frac{\partial}{\partial r}\left(r\frac{\partial \varphi}{\partial r} + reE_r\frac{\varphi}{T}\right) + \xi eE_r\frac{1}{4}\left(\frac{\partial G}{\partial r} + \frac{eE_r}{T^*}G\right) + \frac{1}{4}\xi\frac{(eE_z)^2}{T^*}G - Q_{\mathrm{el}} + Q_{ee} - Q_{\mathrm{inel}}. \quad (6)$$

Here, the following notation is used:

$$\varphi = \int_{\varepsilon^*}^{\infty} f_0(n_e, T_e, T^*)\varepsilon\sqrt{\varepsilon}d\varepsilon, \quad (7)$$

$G = \frac{6n_e(\varepsilon^*)^{3/2}}{\sqrt{\pi}T_e^{3/2}}e^{-\varepsilon^*/T_e} + \frac{\varphi}{T^*}$, and $\xi = \frac{2}{3ma}$, where $a = \frac{\nu}{\varepsilon}$, that is, it is assumed that the cross section for elastic electron-atom collisions is proportional to $\varepsilon^{0.5}$; for argon, we have $a = 1.2 \times 10^9 p$ $(\mathrm{s\ eV})^{-1}$. $Q_{\mathrm{el}}$, $Q_{\mathrm{inel}}$, and $Q_{ee}$ are the terms describing elastic and inelastic losses and the contribution of the electron-electron collisions [11].

Equations (6) and (7) for $\varphi$ were solved numerically by an explicit scheme. Then $T^*$ is calculated using the obtained values of $\varphi$ and definition (7). Thus, Eqs. (2), (6), and (7) for the temperatures $T_e$ and $T^*$ describe the shape of the EEDF for each spatial cell, taking account of the transport of low- and high-energy electrons.

It should be noted that stepwise ionization prevails over direct ionization over almost the entire range of discharge currents. The ionization from excited states is a low-threshold process ($<4$ eV for argon) and its rate coefficient does not vary significantly. Therefore, the variation of the excitation rate coefficient for the lowest metastable levels is the most important. Only high-energy electrons, whose transport is described by the Eqs. (6) and (7) for the temperature $T^*$, are able to excite neutral atoms. Thus, the ionization rate is determined mainly by two parameters: the reduced electric field $E/N$ and the temperature $T^*$, which describes the nonlocal in nonuniform radial field redistribution of the energy between the electrons. Using the solution to the equation for the isotropic part of the EEDF in the local approximation, we obtain the dependence of rate coefficients $k^*(E/N, T^*)$. It should be noted that $k^*$ depends on the reduced electric field and on the temperature of the high-energy part of the EEDF. In turn, $T^*$ depends on the mean electron temperature $T_e$ and degree of ionization $n^e/N$. So we have the following dependence: $k^*(E/N, T^*(T_e, n_e/N))$.

## IV. DIFFUSE, CONSTRICTED, AND CONSTRICTED-STRATIFIED DISCHARGE MODES

### A. Diffuse and constricted discharge modes

First, we will consider D and C discharge modes and the results of systematic calculations for these modes. They are well simulated in local approximation. The developed model has been used for the analysis of experimental data [10], where the glow discharge in tube of radius $R = 1.5$ cm with argon at a pressure of $p = 40-120$ Torr was studied. As mentioned above, such discharges can exist in the following experimental observed [10] modes: D, CS, and C modes. The calculation of the radial distributions of the electron concentration in D mode (discharge current of 10 mA) and C mode (discharge current of 180 mA) at argon pressure of 40 Torr

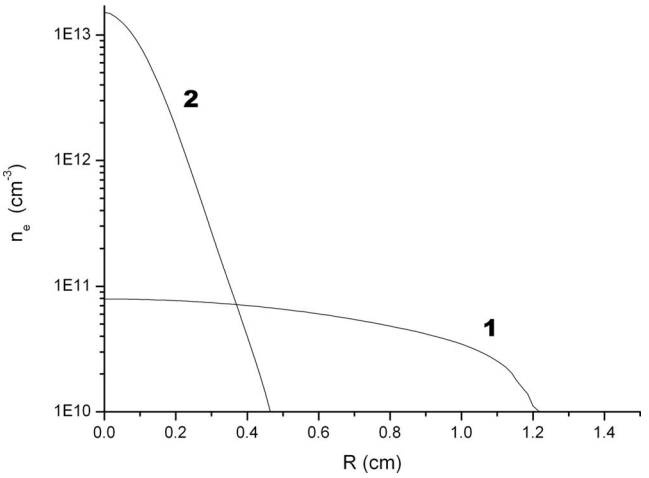


FIG. 1. Radial distribution of the electron concentrations in D (curve 1) and C (curve 2) modes.

are shown in Fig. 1. In the D mode, the radial electron density distribution is close to the Bessel function. In this mode, diffusive losses prevail and the radial distribution of the ionization rate is determined by nonuniform gas heating. Unlike the D mode, where electron density is distributed smoothly along the radius, the electrons in the C mode are mostly concentrated in a narrow near-axis area. As seen in Fig. 1, the current channel shrinks as a result of the constriction and the degree of ionization is increased up to $n_e/N_0 \sim 10^{-5} - 10^{-4}$.

The results of the calculations of the EEDFs in the local approximation at the tube axis ($r=0$) and near the tube wall in the D and C discharge modes are shown in Figs. 2 and 3. In the D mode, the reduced electric field and the electron concentration in the axial region are $E/N=3.7$ Td and $n_e \approx 8\times 10^{10}$ cm$^{-3}$, respectively. These parameters near the wall are as follows: $E/N=1.9$ Td and $n_e \sim 10^8$ cm$^{-3}$. In the D mode, the EEDFs in both regions have a similar shape, which is far from Maxwellian. The high-energy part of the EEDF is depleted due to inelastic electron collisions. In this mode, electron-electron collisions do not affect the EEDF.

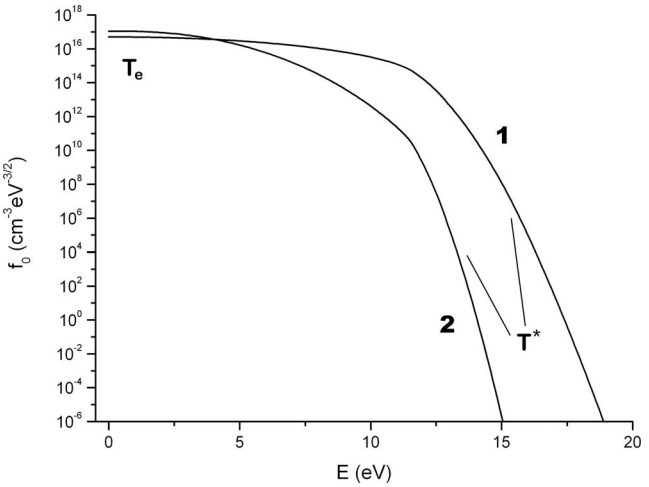


FIG. 2. EEDF at the discharge axis (curve 1) and near the tube wall (curve 2) in the D mode.

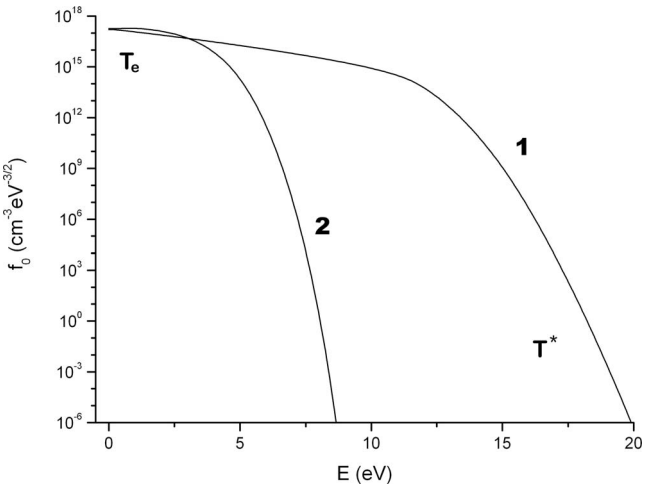


FIG. 3. EEDF at the discharge axis (curve 1) and near the tube wall (curve 2) in the C mode.

The difference between these EEDFs is due to the difference in the $E/N$ values in these regions. The D mode is characterized by the rather high field values and low electron concentrations. On the other hand, the shape of the EEDF in the C mode at the tube axis differs strongly from that near the wall. The relatively low electric field ($E/N<1$ Td) and high electron concentration are typical for a C mode, and therefore the excitation rate coefficients are enhanced by Coulomb interactions between the electrons. Electron-electron collisions influence the EEDF only in the central constricted region. Their influence is nonessential outside this region because of the small degree of ionization. Since the threshold for the excitation of the metastable state of argon is as high as 11.52 eV, the difference between the stepwise ionization rates in the axial region and near the wall is substantial and it determines the pronounced difference in electron concentrations (Fig. 1). In both cases, the EEDFs have a two-temperature shape. This fact with account of the nonlocal formation of the EEDF will be used for the simulation of the hysteresis transition.

The schematic pathway of the transition from the D to the C (CS) mode is shown in Fig. 4. At first, the discharge is in the D mode (point 1). After that, the applied voltage and, as a result, the discharge current are increased instantly (point 2). The increase in the electric field leads to the increase in the electron concentration. In turn, this leads to the decrease in the electric field because of the conservation of the discharge current. At reaching the critical value of the electron concentration ($\sim 5\times 10^{11}$ cm$^{-3}$) the Coulomb interactions between electrons increase significantly the ionization rate. This again leads to the electron concentration growth and decrease in the electric field. After all, the discharge comes to the C mode (point 3). It should be noted that this simulation was carried out in frame of 1D model. In our calculations, at the transition from the D to the CS mode we observe rather slow electron concentration growth until the discharge reached the constricted state. After that the constricted state is destroyed and oscillations are appeared. In the experiments, it was observed that such transition could develop from the cathode to the anode through the entire positive

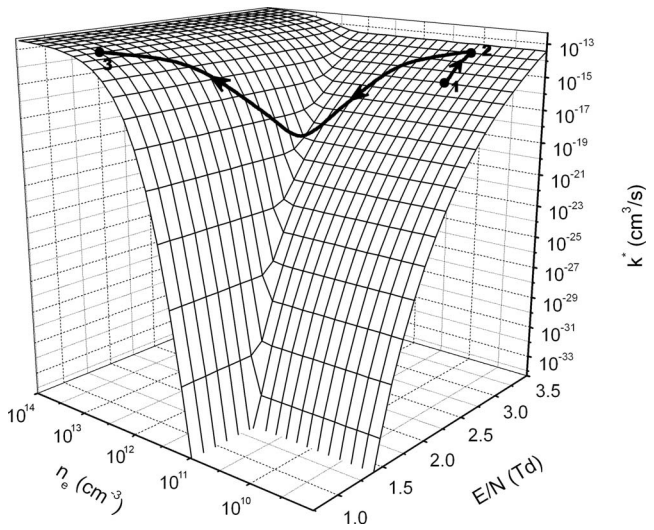


FIG. 4. Excitation rate constant $k^*$ as a function of the electron density and reduced field and the schematic pathway of the transition from the D to the C (CS) mode.

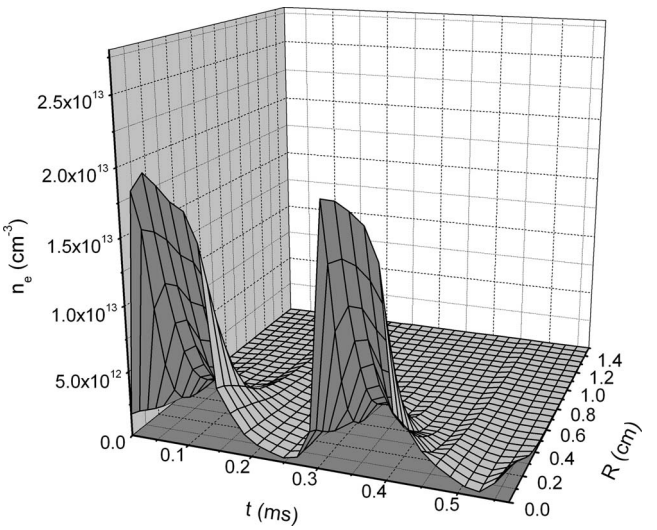


FIG. 5. The radial distribution of the electron concentration as a function of time.

column [33]. The transition in the experiments occurs faster, because at the cathode the instability rather appears, but this should not change significantly the value of the discharge current at which the transition takes place.

### B. Constricted-stratified discharge mode

The results of our calculations of CS mode are presented in this section. As mentioned above, the transition from the D mode to the C mode occurs via CS mode. As a rule, the simulations of the C mode and transition between D and C modes do not take into account an appearance of the oscillations of the plasma parameters at the transition to the C mode. Although, in [10,14] it was shown that in a wide range of discharge currents ($\approx$20–200 mA) constriction of the discharge is accompanied by the appearance of moving striations. The calculated values of the electric field in the C mode were considerably lower than experimental ones. The calculated electric field $E$ in the CS mode should be averaged across the regions with high and low electric fields for comparison with the experimental field $E$ (only for comparison) measured by probe methods or from the total voltage drop on the positive column. The probes measure the voltage drop on the length involving several striations. In [10], the fields in the right part of the CVC apparently correspond to an averaged field value. Paper [10] presents the time dependences of plasma emission for the CS mode, made by a high-speed CMOS camera, at a given point on the tube length.

The developed 1D radial model was applied to study the CS mode. We calculated the radial distributions of plasma parameters and their time behavior. Our calculations show that the plasma parameters do not reach a constricted steady-state regime and show periodic oscillations in this mode. Figure 5 illustrates the radial distribution of electron concentration as a function of time for the experimental conditions given in [10]: $I$=40 mA and $p$=40 Torr. As one can see, this discharge mode has periodic oscillations in time. The nature of these oscillations will be considered below. The period of such oscillations ($\sim$0.25 ms) is comparable with the experimental observed period ($\sim$0.4 ms) of the striations for this mode [10].

To study the nature of such oscillations it is useful to trace the electron temperature $T_e$, the electric field $E$, and the metastable state concentration $n^m$ at the axis as a function of time (Fig. 6). These parameters display well-defined periodic oscillations. One can see that each next oscillation starts from a jump of the electric field, which in turn causes the increase in $T_e$, $E$, and $n^m$. The substantial jump of the electric field $E$ causes an almost immediate reaction in all the other plasma parameters (the typical time taken by the electron process is $\sim 10^{-10}$ s). At the beginning of each striation we can see high peaks in all parameters under study. Further, because of a high concentration of metastable atoms, the growth of the electron concentration is observed. This, in turn, leads to an increase in current density and the electric field decreases to preserve the given discharge current. As a result, the electron temperature and $n^m$ start to decrease. Furthermore, the decrease in the metastable atom concentration is enhanced by the mixing of metastable and resonant levels and radiative decay of the latter. At this time, the electron concentration is still high enough and Coulomb interactions between electrons increase the excitation rates considerably. This explains the sufficiently slow change in the concentrations of electrons and excited atoms. The nonsteady-state C mode exists in this region for some time. It results from the following. The electric field in this mode is very low and Coulomb interactions only redistribute energy between electrons. The electron-energy losses in inelastic collisions are enhanced due $e$-$e$ collisions. At the same time the low electric field does not compensate for these losses and electron temperature $T^*$ starts to decrease. As a consequence, a fast decrease in the excited atom and electron concentrations is observed, and the C mode breaks down. Electron temperature $T^*$ was obtained from Eq. (6) in nonlocal approximation. As it will be shown later, the decay of the constricted state in the CS mode (Fig. 5), as the hysteresis transition, cannot be described in the local approximation.

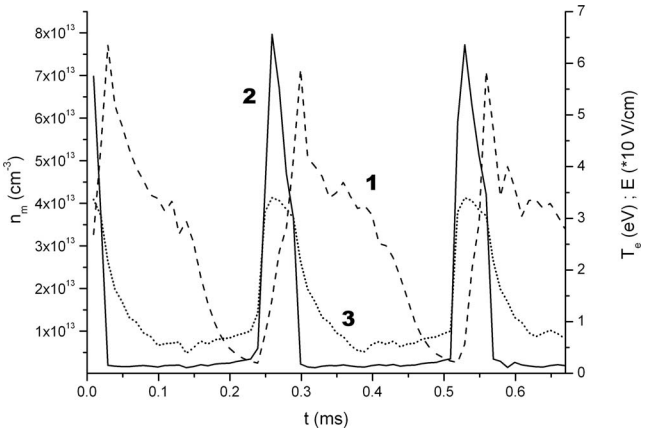


FIG. 6. The concentration of the metastable state (curve 1), electric field (curve 2), and electron temperature $T_e$ (curve 3) at the tube axis as a function of time.

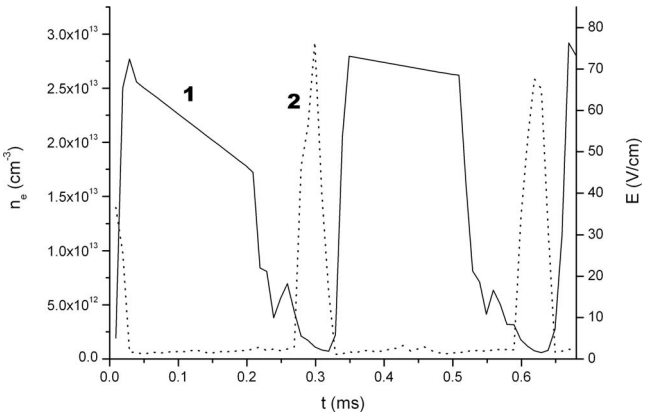


FIG. 7. Electron concentration at the discharge tube axis (curve 1) and electric field $E$ (curve 2) as a function of time.

In our calculations, we did not take into account the nonlocal effects in nonuniform axial field $E$. More correct description of the striations (CS mode) is possible only with a 2D (axis-radial) model. This 2D model could increase the period of such oscillations. Periodic plasma parameter oscillations in a 1D (radial) model can be interpreted as discharge parameter oscillation within a positive column at a given tube cross section. Furthermore, as it was mentioned in [15], there is no basic difference between motionless and moving striations—they are both periodic repetitions of local fluctuations in plasma.

In the CS mode, we can observe the following picture. The electrons first pass the region with a high electric field. Here they gain energy and produce almost no ionization (because of the initial low electron concentration and low electron energy). Then the electron energy is gradually increased and the electrons start to ionize. We can observe the appearance of the region with high electron concentration [and low electric field (striation)]. Here the ionization rate is enhanced due to electron-electron collisions and we observed the simultaneous increase in $n_e$ and fast decrease in $E/N$ (Fig. 5 and 6) to preserve the constant discharge current. As electrons move from cathode to anode, the hot electrons appear from the cathode side and thus the striation head (the region of main ionization) is displaced in direction from the anode to the cathode in noble gases [15]. In the tail of the striation, electrons only lose their remaining energy in inelastic collisions and we can observe the decay of the constricted state.

To confirm our assumptions about the nature of the CS mode we have carried out the calculations for lower pressure discharge ($p=2$ Torr and $I=30$ mA), where the striations without the constriction were observed experimentally [14]. If the oscillations in the S and CS modes occurred by the same reason and our model was not correct, we would obtain oscillations in the S mode. In our calculation, we have failed to obtain oscillations in this mode: the discharge parameters attain the steady-state values. So, it is possible to conclude that the appearance of the striations in the S mode is induced by axial disturbances in nonuniform axial electric field. These conclusions agree with the results presented in [14,34]. The fact that there are periodic plasma parameter oscillations in our calculations for the CS mode while there are no oscillations for the S mode means that these oscillations can be of different natures.

## V. TRANSITIONS FROM THE CONSTRICTED-STRATIFIED TO THE DIFFUSE AND CONSTRICTED DISCHARGE MODES

### A. Transition between CS- and C-discharge modes

Now we will analyze the variations of the plasma parameters with the discharge current at the transition from CS to C mode. At extremely high currents (in the case under study, 180 mA and higher) the discharge passes smoothly from the CS mode into the C mode. To study such a transition the calculations for the CS mode were carried out at various discharge currents: 70, 120, 150, 180, and 250 mA. Figures 7 and 8 show electron concentration, temperatures $T_e$ and $T^*$, the electron concentration $n_e$, and electric field $E$ at the discharge tube axis as a function of time at the discharge current value of 70 mA.

Figures 5 and 7 show that the period of plasma parameters oscillation increases with the discharge current. As all the

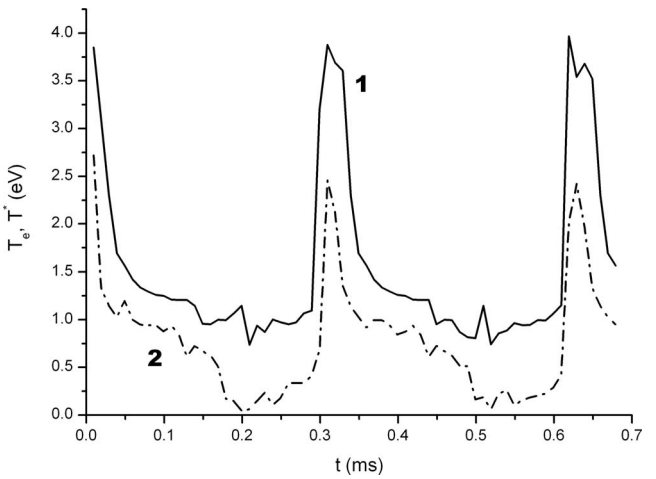


FIG. 8. Electron temperatures $T_e$ (curve 1) and $T^*$ (curve 2) as a function of time.

striations in noble gases are moving, we can refer to a length of this region when we are speaking about the duration of the phase of high or low electron number density. In the CS mode, an increase in the discharge current leads to an increase in the period of oscillations. Thus the increase in the length (duration) is specific to the region with the high electron concentrations (such as regions at $t \sim 0-0.2$ and 0.35–0.5 ms in Fig. 7) and the length of the region with low electron concentration decreases. Since the electric field in the regions of high electron concentrations is higher at higher discharge currents, the electron temperature $T_e$ is higher as well. However, that is still not enough for the steady-state existence of the discharge in the C mode, and after a while, when the energy gathered by electrons is dissipated, their concentration will start to fall again. Figure 7 shows that after the fall in the electric field, the electron temperature will fall as well, but not as much as it does at a current of 30 mA. This is because the electric field here is higher and electrons gather energy (although not very much) in the region with high electron concentration.

Now, let us consider the decay of the C mode (the decay of striation in the CS mode). The electrons intensively gain the energy in the high electric field region. The gain of this energy induces the increase in $T^*$. As mentioned above, they produce the main ionization at the head of the striation. While the electric field falls (in the beginning of the striation), the electron concentration does not fall yet. Figure 8 shows that the intense energy redistribution between electrons (electron-electron collisions) starts in the region of elevated electron concentrations and degraded electric fields. At some stage (e.g., $t \approx 0.35-0.5$ ms) $T^*$ remains quite high ($T^* \approx 1.0-0.07$ eV) while $T_e$ falls ($T_e \approx 1.75-0.75$ eV). This indicates the energy redistribution between electrons. Electrons, colliding with each other, transfer part of their energy into the EEDF's tail from the EEDF's body. Since the number of high-energy electrons is less than the general number of electrons, this process takes place for some time. But at this stage, nonetheless, electrons cannot gain energy efficiently in the region of low fields. The high ionization rate leads to the decrease in $T_e$. When the value of $T_e$ becomes equal to $T^*$, a sharp decrease in $T^*$ is observed and the C mode decays.

The lowest level of electric fields in the region of high electron concentrations is increased with the discharge current, and electrons can gain more energy in this region at high discharge currents. As a result, the decrease in electron temperature $T_e$ slows down at higher discharge currents and the duration of the phase of high electron concentrations increases. Thus, the increase in the striation length is observed: the higher the discharge current, the greater the length of the region of high electron concentrations and the smaller the intervals between such regions. At the critical discharge current value, the field in the striation (the region of high $n_e$) is sufficient to maintain a steady-state C mode.

### B. Hysteretic transition between D- and CS-discharge modes

As mentioned above the schematic transition from the D mode to the C (CS) mode is shown in Fig. 4. The reverse transition from C (CS) mode to the D mode is more complex (nonlocal) and cannot be shown in the frame of the $n_e$ and $E/N$ local dependence of the excitation rate coefficient. Here we present the results of calculations of the hysteresis transition from CS mode to the D mode. We carried out systematic calculations of the transition between D and CS modes of the discharge. This transition is interesting for two reasons: first, at this transition the phenomenon of a hysteresis in the CVC is observed; and second, it is a serious problem for discharge models to obtain a decay of the C mode and a disappearance of the oscillations at the transition to the D mode. In our case, the discharge transition from the CS to D mode deals with the effects of the radial nonlocal formation of the EEDF [11]. They are the same as in [11]. But in [11] the oscillations were suppressed, and only the mechanisms taking out the discharge from the constricted mode were under study. We have obtained the oscillations (which are called in [14] as a CS mode) both in Ar and Ne. The principal behavior of oscillating plasma parameters was similar in both gases. Here we are focused on the results for the argon plasma. So this section presents the results of our simulation of the hysteresis transition between D and CS modes (which has a complex structure). It should be noted that this radial nonlocality of the EEDF tail is of a different kind than the axial nonlocality of the EEDF tail considered in [14,34] used for the description of the pure striations (S mode).

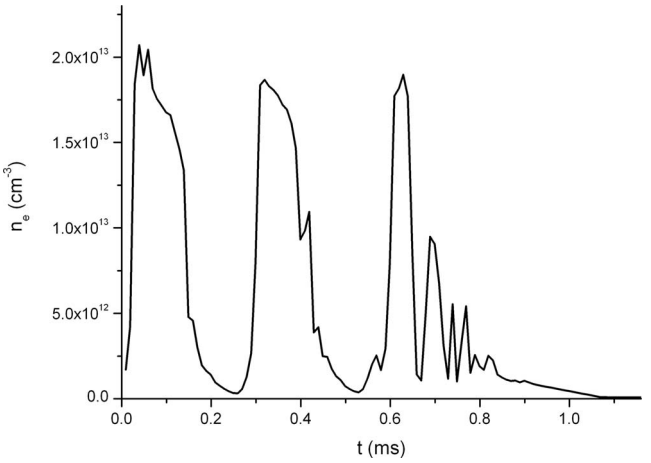


FIG. 9. Electron concentration at the tube axis as a function of time at the transition from the CS mode to the D mode.

Figure 9 illustrates the discharge transition from the CS mode to the D mode. Here the electron concentration at the tube axis as a function of time is shown. At the initial stage ($t < 0.6$ ms) the discharge is in the CS mode at a current of 30 mA. Then, the discharge current value is reduced smoothly until it becomes equal to 17 mA at $t=0.75$ ms. It can be seen that the amplitude and period of oscillations decrease with the decrease in the discharge current. The most evident illustration of this transition is shown in Fig. 10, which displays the radial profiles of the temperature of the EEDF's high-energy part in the CS mode in the region with high electron concentration at various values of the discharge current: the discharge current is lower; the central hot area is narrower. When reaching the critical value of the discharge current (17 mA), the $T^*$ radial profile width becomes less

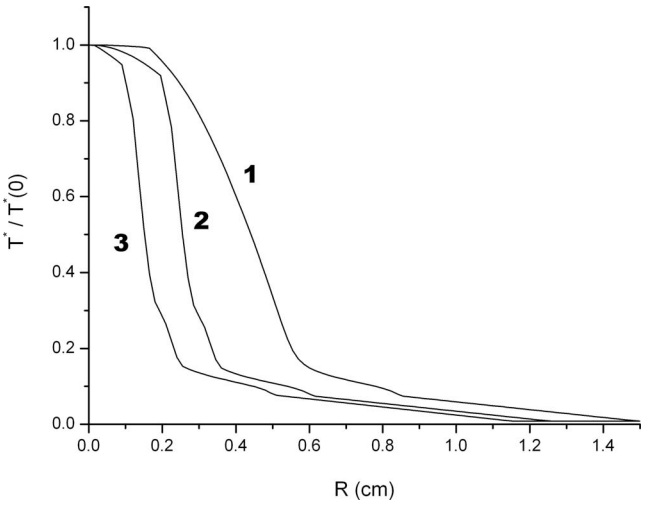


FIG. 10. Radial profiles of the normalized temperature $T^*$ of the high-energy part of the EEDF in the CS mode in the region with high electron concentration at various values of the discharge current: 1–30, 2–20, and 3–17 mA.

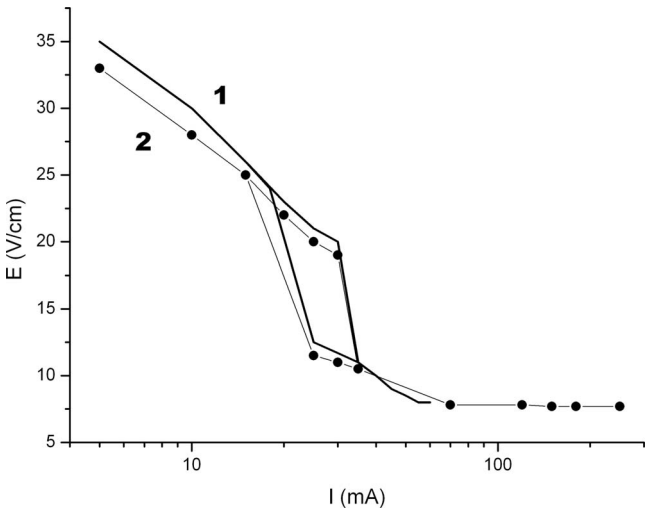


FIG. 11. Current-voltage characteristic of a dc discharge in argon: experiment [10] (curve 1) and 1D model (curve 2).

than the electron-energy relaxation length. The profile cannot become any narrower. At the transition to the D mode, the hot electrons diffuse effectively from the central hot region since the $T^*$ radial profile width is less than the electron-energy relaxation length. This results in switching off the effect of the EEDF Maxwellization and ionization rate depending mainly on the reduced electric field. This means that as the discharge relaxes to a steady state it passes into the D mode without discharge plasma parameter oscillations.

In our simulations, the following picture was observed in the local approximation. If the discharge is in the CS mode, then, as the discharge current is decreased below the value of the discharge current at which the transition to the D mode takes place in the experiment, the system remains in a constricted state and the discharge channel narrows to less than four grid cells (in our simulations, the radial size of the grid cell was 0.15 mm). In this case, the simulation results lose their physical meaning, because the transition or the absence of a transition is determined by numerical effects and the size of the grid cell. Taking into account the emission and reabsorption of resonant radiation would insignificantly affect the radial profiles of the charged particle densities. At the discharge axis, the excitation rate coefficients are very high and, as it was mentioned, the rate of ionization from the resonant level is higher than the radiative rate for this level. Radiation emitted from the discharge channel increases the concentration of $Ar^r$ in off-axis regions. However, this does not lead to a considerable increase in the ionization rate beyond the discharge channel, because, in the CS mode, at currents lower than the critical value, the electron concentrations there are very low. Weak ionization that can take place in this region is balanced by the higher recombination rate (molecular ions prevail in this region).

As the transition from the CS mode to the D mode is determined by nonlocal effects (not local parameters such as reduced electric field and electron concentration), the critical value of the discharge current (at which the transition to the D mode takes place) is also determined by nonlocal effects (as distinct from the transition from D to the CS mode). And calculations show, that the jumplike transition from the CS to the D mode occurs at a lower discharge current than that of the reverse transition from the D to the CS mode.

However, it must be noted that the decrease in current also causes a decrease in the oscillation period. Thus, the wavelength becomes comparable to the electron-energy relaxation length. It is possible that the transition occurs a little earlier because of the longitudinal nonlocal effects. The experimental value of the critical current is 20–25 mA. In our calculations, this value was ~17 mA, which is quite close to the experimental value. This means that longitudinal effects can be important along with radial nonlocal effects.

Figure 11 shows the calculated CVC characteristics of a dc discharge in argon in the experimental conditions [10]. The characteristic demonstrates a well-pronounced hysteresis effect. The value of the electric field on the left part of this curve (after the hysteresis transition) is the field averaged across the regions with high and low electric fields. It presents all three simulated modes: the D mode on the left part of the CVC characteristic before the jump ($I < 17-33$ mA), the CS mode ($33 < I < 180$ mA), and the C mode ($I > 180$ mA). No abrupt transitions are observed during the transition from the CS to the C discharge modes. To the best of our knowledge, until now there have been no publications in which the hysteresis transition between the D and CS discharge modes was obtained numerically. It is seen that the CVC calculated reproduces the measured one and that both the direct transition from the D to the CS mode and the reverse transition occur at the same values of the discharge current as in the experiment [10]. This indicates that the model correctly takes into account the basic processes leading to the discharge CS mode and bringing the system out of the CS mode.

## VI. CONCLUSIONS

The 1D self-consistent model was applied to study high-pressure dc discharges in noble gases. Three discharge

modes were considered: D, CS, and C modes. The periodic oscillations of plasma parameters in the CS mode were observed during calculation in our model. It was shown that the oscillations in this mode are different to the oscillations in the S mode. It was revealed that radial nonlocal effects of electron kinetics in the axial electric field lead to the electron concentration oscillations and formation of the periodic structures with high field domains. These oscillations are caused by the inconsistency between the electron-energy losses and gains in the axial electric field in the conditions of radial nonuniformity of plasma parameters. The values of the axial electric field averaged across the regions with high and low electric fields are very close to the experimental values. The discharge operates in the C mode at discharge currents higher than the critical value.

The transitions between these discharge modes were studied using the developed model. A transition from the D to the CS mode occurs by a jump and is accompanied by a hysteresis effect. It was shown that the experimentally observed hysteresis of the CVC at the transition between the CS and D modes deals with the nonlocal formation of the EEDF, namely, the diffusion of high-energy electrons from the central constricted region. The effect of the nonlocal formation of the EEDF was taken into account by introducing the effective temperature of the high-energy part of the EEDF and solving the equation for the radial profile of this temperature. The developed model made it possible to obtain direct and reverse (from the CS mode to the D mode) transitions very similar to the experimentally observed CVC. At high discharge currents, the calculated transition from the CS mode to the C mode occurs smoothly without any jumps.

## ACKNOWLEDGMENT

We are pleased to acknowledge support from the RF Government for Key Science Schools Grant No. 133.2008.2.

[1] Yu. P. Raizer, *Gas Discharge Physics* (Nauka, Moscow, 1987/ Springer-Verlag, Berlin, 1991).
[2] *Encyclopedia of Low-Temperature Plasma*, edited by V. E. Fortov (Nauka, Moscow, 2000), Vols. 1 and 2.
[3] E. P. Velikhov, A. S. Kovalev, and A. T. Rakhimov, *Physical Phenomena in Gas Discharge Plasma* (Nauka, Moscow, 1987).
[4] A. P. Napartovich and A. N. Starostin, in *Plasma Chemistry*, edited by B. M. Smirnov (Atomizdat, Moscow, 1979), Vol. 6, p. 153.
[5] Yu. B. Golubovskii and R. Sonnenburg, Zh. Tekh. Fiz. **49**, 295 (1979) [Tech. Phys. **24**, 177 (1979)].
[6] Yu. B. Golubovskii and R. Sonneburg, J. Phys. Colloq. **40**, C7–155 (1979).
[7] Yu. B. Golubovskii, V. O. Nekuchaev, and E. B. Pelyukova, Zh. Tekh. Fiz. **66**, 43 (1996) [Tech. Phys. **41**, 254 (1996)].
[8] Yu. B. Golubovskii, V. O. Nekuchaev, and E. B. Pelyukova, Zh. Tekh. Fiz. **66**, 76 (1996) [Tech. Phys. **41**, 1011 (1996)].
[9] G. M. Petrov and C. M. Ferreira, Phys. Rev. E **59**, 3571 (1999).
[10] N. A. Dyatko *et al.*, J. Phys. D **41**, 055204 (2008).
[11] I. A. Shkurenkov, Yu. A. Mankelevich, and T. V. Rakhimova, Plasma Phys. Rep. **34**, 780 (2008).
[12] J. Gunn, Solid State Commun. **1**, 88 (1963).
[13] J. Goldman, D. C. Tsui, and J. E. Cunningham, Phys. Rev. Lett. **58**, 1256 (1987).
[14] V. I. Kolobov, J. Phys. D **39**, R487 (2006).
[15] L. Pekarec, Usp. Fiziol. Nauk **94**, 463 (1968).
[16] Yu. B. Golubovskii, V. A. Maiorov, V. O. Nekutchaev, J. Behnke, and J. F. Behnke, Phys. Rev. E **63**, 036409 (2001).
[17] I. A. Shkurenkov, Yu. A. Mankelevich, and T. V. Rakhimova, J. Phys.: Conf. Ser.(2009) (to be published).
[18] L. M. Chanin and M. A. Biondi, Phys. Rev. **106**, 473 (1957).
[19] V. Lj. Marković, S. R. Gocić, S. N. Stamenković, and Z. Lj. Petrović, Phys. Plasmas **14**, 103504 (2007).
[20] A. V. Phelps, JILA Information Center Report No. 28, 1985 (unpublished), http//jilawww.colorado.edu/avp/collisiondata
[21] K. Tachibana and A. V. Phelps, Phys. Rev. A **36**, 999 (1987).
[22] K. Tachibana and A. V. Phelps, Phys. Rev. A **37**, 1786 (1988).
[23] *Handbook of Physical Data*, edited by I. S. Grigoriev and E. Z. Meilihov (Energoatomizdat, Moscow, 1991).
[24] B. M. Smirnov, *Ions and Excited Atoms in Plasma* (Atomizdat, Moscow, 1974).
[25] V. S. Marchenko, Zh. Eksp. Teor. Fiz. **85**, 500 (1983) [Sov. Phys. JETP **58**, 292 (1983)].
[26] E. W. McDaniel, *Collision Phenomena in Ionized Gases* (Wiley, New York, 1964/Mir, Moscow, 1967).
[27] L. M. Biberman, V. S. Vorob'ev, and I. T. Yakubov, *Kinetics of Nonequilibrium Low-Temperature Plasmas* (Nauka, Moscow, 1982/Consultants Bureau, New York, 1987).
[28] V. A. Ivanov, J. Phys. B **31**, 1765 (1998).
[29] V. I. Kolobov and R. R. Arslanbekov, IEEE Trans. Plasma Sci. **34**, 895 (2006).
[30] I. P. Shkarofsky, T. W. Johnston, and M. P. Bachynskii, *The Particle Kinetics of Plasmas* (Addison-Wesley, Reading, MA, 1966/Atomizdat, Moscow, 1969).
[31] V. A. Feoktistov, A. M. Popov, O. B. Popovicheva *et al.*, IEEE Trans. Plasma Sci. **19**, 163 (1991).
[32] V. L. Ginzburg and A. V. Gurevich, Usp. Fiziol. Nauk **70**, 201 (1960) [Sov. Phys. Usp. **3**, 115 (1960)].
[33] A. Garscadden, P. Bletzinger, and T. C. Simonen, Phys. Fluids **12**, 1833 (1969).
[34] L. D. Tsendin, Plasma Sources Sci. Technol. **4**, 200 (1995).